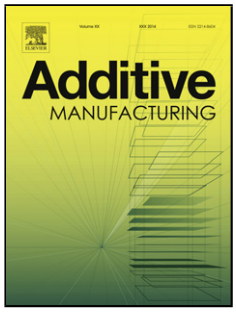

Title: Crack propagation and fracture toughness of Ti6Al4 V alloy produced by selective laser melting

Author: V. Cain L. Thijs J. Van Humbeeck B. Van Hooreweder R. Knutsen

PII: S2214-8604(14)00030-X
DOI: http://dx.doi.org/doi:10.1016/j.addma.2014.12.006
Reference: ADDMA 23

To appear in:

Received date: 25-7-2014
Revised date: 27-11-2014
Accepted date: 12-12-2014

Please cite this article as: Cain V, Thijs L, Van Humbeeck J, Van Hooreweder B, Knutsen R, Crack propagation and fracture toughness of Ti6Al4<ce:hsp sp=Ö.25Ï>V alloy produced by selective laser melting, *Addit Manuf* (2014), http://dx.doi.org/10.1016/j.addma.2014.12.006

Crack propagation and fracture toughness of Ti6Al4V alloy produced by selective laser melting

V Cain[a,b], L Thijs[c], J Van Humbeeck[c], B Van Hooreweder[d] and R Knutsen[a]

[a]*Centre for Materials Engineering, Department of Mechanical Engineering, University of Cape Town, South Africa*

[b]*Department of Mechanical Engineering, Cape Peninsula University of Technology, South Africa*

[c]*Department of Metallurgy and Materials Engineering, KU Leuven, Kasteelpark Arenberg 44, B-3001 Leuven, Belgium*

[d] *Department of Mechanical Engineering, KU Leuven, Celestijnenlaan 300b, B-3001 Leuven, Belgium*

Corresponding author; *V.Cain*

E-mail: *cainv@cput.ac.za*

Ph: +2721 650 3173

Abstract

The fracture toughness (K_{1c}) and fatigue crack growth rate (FCGR) properties of selective laser melted (SLM) specimens produced from grade 5 Ti6Al4V powder metal has been investigated. Three specimen orientations relative to the build direction as well as two different post-build heat treatments were considered. Specimens and test procedures were designed in accordance with ASTM E399 and ASTM E647 standard. The results show that there is a strong influence of post-build processing (heat treated versus 'as built') as well as specimen orientation on the dynamic behaviour of SLM

produced Ti6Al4V. The greatest improvement in properties after heat treatment was demonstrated when the fracture plane is perpendicular to the SLM build direction. This behaviour is attributed to the higher anticipated influence of tensile residual stress for this orientation. The transformation of the initial rapidly solidified microstructure during heat treatment has a smaller beneficial effect on improving mechanical properties.

Keywords: Selective laser melting, Ti6Al4V, fracture toughness, fatigue crack growth rate, microstructure

1. Introduction

Selective laser melting is an additive fabrication process in which successive layers of powder are selectively melted by the interaction of a high energy density laser beam. Molten and re-solidified material forms parts, while non-melted powder remains in place to support the structure [1]. This layer-wise production technique offers some advantages over conventional manufacturing techniques such as high geometrical freedom, short design and manufacturing cycle time and made-to-order components. Layer-wise production techniques have evolved rapidly in the last 10 years and SLM has changed from a rapid prototyping to an additive manufacturing technique. Consequently, the static and dynamic material properties must be sufficient to meet in service loading and operational requirements. It is well known that the SLM process is characterized by high temperature gradients leading to rapidly solidified, non-equilibrium microstructures [2]. High localised thermal gradients and very short interaction times, which leads to rapid volume changes, causes substantial residual

stress development. Furthermore, the option of changing the process parameters can have a strong influence on the microstructure, density and surface quality. As a result, the mechanical properties of SLM parts can differ substantially from one another and from those produced by conventional techniques. In this respect it is recognised that the advantages of SLM can only be realised when the mechanical behaviour of the final products is at least able to be matched to conventionally produced components of the same material.

In recent years, much research has focused on optimising the SLM process. Kruth et al. [3] concentrated on studying the SLM part and material properties specifications in order to improve the quality of the resulting products. In another study Yasa et al. [4] focused on how the mechanical properties obtained with SLM may differ from the ones of bulk material. At present, Ti-alloys can be processed with high repeatability and hence low variation in material density and mechanical properties. Vilaro et al. [5] studied the effect of applying specific heat treatments to SLM produced Ti6Al4V in order to produce a preferred final microstructure. Furthermore Thijs et al. [2] concentrated on the effects on density that varying scanning parameters and scanning strategies could have. Moreover, quasi-static material properties such as tensile strength, hardness, and impact toughness have been well characterised [3] and are reported to match those of conventional wrought materials. On the other hand, substantial complexities arise when attempting to characterise the dynamic mechanical behaviour since crack initiation and propagation is critically sensitive to the interaction between fracture path, orientation, microstructure and loading conditions. In addition, residual stresses which arise as a result of the rapid localised temperature fluctuations during the

SLM process strongly influence crack initiation and growth. A previous study has shown that these residual stresses have detrimental effects on the mechanical behaviour of SLM parts [6]. The knowledge of these properties and the underlying failure mechanisms remains limited, and consequently there is insufficient confidence in being able to predict fatigue life. Nevertheless, a few studies have reported the potential for SLM parts to meet the fatigue life requirements. In a study by Van Hooreweder et al. [1], nearly fully dense (>99%) SLM-Ti6Al4V specimens were produced with fracture toughness and fatigue crack growth properties similar to those of mill annealed vacuum arc remelted (VAR) Ti6Al4V parts. More recently, a study by Leuders et al. [7] investigated the influence of two building orientations and three post-build treatments. The post-build annealing treatments were performed at 800° and 1050°C (for 2 hours) and a hot isostatic pressing (HIP) process was performed at 920°C at a pressure of 1000 bar for 2 hours. All specimens were furnace cooled. Although residual porosity was noted to assist crack growth, residual stresses and their subsequent elimination proved to have a substantial influence on fatigue properties. The post-build annealing treatments in the range 800°-1050°C not only relieve residual stress, but also modify the as-built rapidly solidified microstructure which comprises of fine acicular martensite (α' phase). The latter microstructure is highly directional as a result of the imposed solidification mode during the vertical layer by layer build process. The purpose of the annealing treatment is to generate the preferred lamellar $\alpha+\beta$ equilibrium structure which provides a more desirable combination of strength and toughness. However, it is important that the annealing treatment does not result in excessive grain growth as was reported by Vrancken et al. [8] when heat treating above the β transus temperature and Leuders et al. [7] for the annealing treatment at 1050°C.

The present work considers different post-SLM processing heat treatment compared to those studied by Leuders et al. [7] and introduces a third building orientation in order to more comprehensively evaluate the influence of anisotropy on mechanical properties. Post-SLM processing heat treatment is directed at reducing residual stress and transforming the as-built martensitic microstructure. In this regard, stress relief heat treatment has been performed at 650°C whereas for the annealing heat treatment, specimens were soaked at 890°C. The maximum annealing heat treatment temperature does not exceed the β-transus temperature as advised in the work of Vrancken et al. [8]. Furthermore only material with >99% density has been evaluated. The mechanical properties, including tensile, fracture toughness and fatigue crack growth rate measurements, were determined for the as-built (AB), stress relieved (SR) and annealed (HT) conditions.

2. Materials and Methods

2.1 Materials

Standard tensile and compact-tension (CT) specimens were manufactured from grade 5 Ti6Al4V spherical powder for the determination of tensile, fracture toughness (K_{1c}) and fatigue crack growth rate (FCGR) properties. The powder particle size ranged between 15μm and 45μm. Figure 1 designates the bi-directional scanning strategy (x-y plane) and the Z-axis building direction that was used to produce all specimens via the SLM process. After scanning the perimeter, the first layer is scanned in zigzag formation and each scanning direction for the successive layer is rotated by 90°.

The full set of tensile specimens and the CT specimens were manufactured respectively in one build-platform to avoid potential variances associated with powder quality. The orientation of the CT specimens on the build-platform, as well as their geometry, is shown in Figure 2 (a, b).

For the determination of K_{1c}, the thickness of the sample, *B* is equal to 12.5 mm, whilst FCGR specimens have a thickness *B* equal to 6.25 mm. Other than this difference in *B* value, specimens have the same geometry. The crack length is specified as *a*. The dimensions of the test specimens are similar to the ones applied in a previous study by Van Hooreweder et al. [1]. The CT specimens in Figure 2(a) are labelled according to ASTM E399 standard: axis direction perpendicular to the notch plane followed by the axis direction in which the crack is expected to propagate. Consequently, three different specimen geometries arise, namely XZ, ZX and XY. The XZ and ZX specimens were built individually on the platform whereas for the XY specimens a continuous block extending in the Z direction was produced from which the individual specimens were later sliced by electric discharge machining (EDM). In all cases the specimens were slightly oversized and were machined to final dimensions prior to mechanical testing. The crack notch was machined by EDM. The machined surface roughness (Ra) was measured using an optical profilometer and in all cases the Ra values conformed to the ASTM E399 and ASTM E647 standards. The density was measured for all the specimens using the Archimedes method which indicated > 99% density in all cases. The SLM build approach for the tensile specimens was the same as the CT specimens and the two test orientations are indicated in Figure 3. Similar density to the CT specimens was recorded.

2.2 Heat treatment

In the case where heat treatment was applied to the as-built specimens, two different processes were considered. For the stress relief (SR) treatment, specimens were soaked at 650 ˚C for 4 hours. The annealing treatment was performed at 890 ˚C for 2 hours and was based on the work by Vrancken et al. [8]. All heat treatments were carried out in a horizontal tube furnace under a protective argon atmosphere and specimens were furnace cooled. Heat treatments were performed prior to final machining.

2.3 Mechanical testing

Tensile testing, fracture toughness (K_{1c}) and FCGR measurements were performed for the respective AB, SR and HT conditions and three specimens were evaluated for each test variable. Tensile tests were performed according to ASTM E8/E 8M standard. The growth of pre-cracks and the measurement of FCGR was performed on a 160 kN Schenk servo-hydraulic machine. For the preparation of pre-cracks, a 7 mm long pre-crack was developed at the notch root by fully reversed cyclic loading at 7 Hz. The crack length was monitored visually using a camera system. After pre-crack development, fracture toughness was measured in tension at a displacement speed of 1 mm/min until failure of the specimen occurred. The fracture toughness test conditions adhered to the ASTM E399 standard. Pre-crack lengths were confirmed after fracture using a Mitutoyo non-contact precision optical measuring system.

Fatigue crack growth rate (FCGR) experiments were carried out according to the ASTM E647 standard. Prior to commencing the FCGR evaluation, a 1mm long pre-crack was developed at the notch root by fully reversed cyclic loading at 5 Hz. The actual FCGR was determined using a cyclic load in tension (R = 0.1) with a fixed amplitude ΔP and a fixed cycle frequency of 5 Hz. The crack propagation was monitored visually with the aid of a camera system and the raw data was translated to a crack length (a) versus number of cycles (N) curve. Due to the visual nature of the measuring technique there exists the possibility of a slight error in readings (up to 5%). The da/dN ratios were then calculated for each curve and ΔK values were determined. The Paris parameters C and m were determined from the da/dN versus ΔK plot according to the Paris equation.

The microstructure of the AB, SR and HT conditions was examined by preparing metallographic sections perpendicular and parallel to the SLM build direction (Z-axis) in order to account for the anisotropic grain growth during the SLM process. The metallographic specimens were etched after conventional grinding/polishing in a mixture of 100 ml distilled water, 2 ml HF and 5 ml HNO_3 (Krolls reagent) and they were examined using brightfield light microscopy.

3. Results

3.1. Tensile testing

The tensile mechanical properties of the material are shown in Figure 4 and are listed in Table 1. No significant difference was observed between the XY an XZ specimen orientations. Very little necking of the specimens was noticed during testing.

The AB tensile specimens showed an average ultimate tensile strength of 1248 MPa with an average elongation at failure of about 6 %. After applying the SR heat treatment at 650˚C the average ultimate tensile strength dropped to 1171 MPa with a slight increase in elongation at failure. In the case of the high temperature annealing heat treatment at 890˚C (HT condition), the average ultimate tensile strength further decreased quite substantially to just below 1000 MPa whilst the elongation at fracture surprisingly also reduced.

3.2 Fracture toughness

Table 2 summarises the K_{1C} values for the three different AB, SR and HT conditions for the respective specimen orientations. In most cases post-SLM processing heat treatment increases the fracture toughness of the material with the largest difference illustrated by the ZX orientation. It is worth pointing out that the pre-crack for the AB specimens in the ZX orientation demonstrates an undesirable crack front (Figure 5) compared to the classical thumbnail crack profile in Figure 6.

3.3 Crack propagation

The results of the FCGR experiments are represented by the Paris curves shown in Figure 7. Figure 7 (a) - (c) displays the effect of specimen process condition for each specimen orientation, whereas Figure 7 (d) - (f) shows the effect of specimen orientation for each specimen process condition. It must be noted that the experimental work did not include the determination of the threshold Δ K values.

For the XY specimen orientation the AB condition shows the slowest crack propagation, whereas the SR condition demonstrates the fastest crack propagation. For the XZ orientation it is clear that the worst case crack growth rates are found for the specimens in the AB condition. For the HT and SR condition there is no noticeable difference between their FCGR behaviour. Similarly, for the ZX specimen orientation the highest crack growth rates are observed for the AB condition. Overall it is shown that the AB condition of the XZ and ZX specimens exhibit the highest crack growth rates, while for the HT condition not only is the behaviour better than the AB condition, but the spread is smaller (Figure 7(f)). The resulting Paris exponents (m), the Paris crack growth rate constants (C) and the correlation factor (R^2) between data and linear fit is tabulated for all of the specimens in Table 3. The correlation factor improves when specimens have undergone a post processing treatment, inferring that there is more scatter in the AB data relative to the SR and HT data. The greater scatter for the AB data could be a result of the variable residual stress distributions introduced by the SLM process.

3.4 Microstructure

The bi-directional scanning strategy is clearly recognisable from the checkerboard pattern displayed by the plane (XY) perpendicular to the build direction (Z-axis) as indicated in Figure 8.

The microstructure parallel to the build direction is indicated in Figure 9.

As is common for the SLM production of Ti6Al4V specimens, a columnar grain structure is clearly visible which arises as a result of the epitaxial growth caused by the successive layer deposition. The heat treatments in this study were designed to avoid significant grain growth by maintaining the maximum temperature below the β-transus temperature (approximately 1000°C).

The metal powder solidifies to form the β phase which subsequently transforms during cooling. Closer inspection of the microstructure in Figure 10 (a) exhibits the martensitic morphology consisting of fine α' plates. When heated to 650˚C (SR condition) the AB martensitic structure partially decomposes towards acicular α as indicated by the slight coarsening seen in Figure 10(b). On the other hand, when heated to 890˚C (HT condition) the reformed β phase upon subsequent cooling forms the Widmanstätten α/β structure shown in Figure 10(c).

4. Discussion

The ultimate tensile strength and yield strength are substantially reduced after heat treatment relative to the AB condition. This behaviour is consistent with the transformation of the initial α′ martensite structure. The more relaxed and coarser microstructure constituents associated with the Widmanstätten morphology in the annealed HT condition results in the lowest strength. However, unlike the findings of Leuders et al. [7] where the elongation at fracture was increased by nearly an order of magnitude (from 1.5% to 11.6%) after annealing at 1050°C, there was very little change in tensile ductility in our case. This may be due to the better initial AB ductility and the

lower annealing temperature compared to the test conditions imposed by Leuders et al. [7].

In the as-built (AB) condition the fracture toughness (K_{1c}) is highest for the XY specimens (28MPa.$m^{½}$) and decreases for the XZ specimens (23MPa.$m^{½}$) with the lowest values recorded for the ZX specimens (16MPa.$m^{½}$). The fact that the same microstructure constituents exist in all the specimens suggests that microstructure anisotropy and/or residual stress anisotropy plays critical roles in controlling the fracture toughness behaviour of the differently oriented specimens. If microstructure morphology only is considered, then it may be expected that the lowest fracture toughness should be demonstrated by the XZ specimen orientation since the crack path cleaves down the length of the columnar grains (akin to chopping wood along the grain). In comparison, the ZX specimen might be expected to display the highest fracture toughness since the crack path is perpendicular to the columnar grain structure whereas the XY specimen could behave in a somewhat intermediate fashion. However, the actual results are quite different to this argument. When residual stress is considered, there are two strong indicators to suggest that the ZX specimen should demonstrate the lowest fracture toughness. In the first instance, the study by Rangaswamy et al. [9] concerning the measurement of residual stresses in AISI316 stainless steel and Inconel 718 samples produced by a similar net-shaping process, indicates that the residual stresses are practically uniaxial with high stresses in the growth (Z) direction. More particularly, their study shows very low residual x- and y-component stresses whereas the residual z-component stress is compressive up to values approximating 400MPa. Of course compressive residual stress will enhance fracture

resistance when the stress is acting to close to the crack, but Rangaswamy et al. [9] have shown that a profile of the z-component stress across the x- and y-directions manifests in high tensile z-component stresses close to the specimen free surfaces in each case (up to 200 MPa). This means that for the ZX specimen, the residual stress along the specimen centre-line may act to reduce the applied tensile load, but the tensile residual stresses near the lateral edges (free surfaces) of the fracture plane will substantially add to the applied tensile load thereby giving rise to a reduction in fracture toughness. This leads to the second indicator which may be argued to account for the lowest fracture toughness for the as-built (AB) ZX specimen. Figure 5 displays an unfavourable pre-crack front for the ZX specimen where the crack is longer close to the free surfaces compared to the specimen centre-line. This particular crack morphology can be accounted for by applying the same deductions illustrated above for the residual stress measurements presented by Rangaswamy et al [9]. In fact, recent analysis by Vrancken et al. [10] using the contour method for measuring the residual stress in the fracture plane supports the presence of high tensile residual stress around the perimeter of the (AB) ZX specimens. Due to the fact that the intention of SLM is to manufacture net shape parts it is not viable to machine or cut away part of the component that might relieve some of the residual stresses. If one then combines the suggested contributions of the microstructure morphology and the residual stress condition, it is reasonable to expect that the (AB) ZX specimen orientation could possess the lowest fracture toughness (dominated by tensile residual stresses perpendicular to the fracture plane near the free surfaces) despite the favourable grain orientation relative to the crack path. The residual stress condition relative to the fracture plane, for reasons interpreted from the work of Rangaswamy et al. [9] and Vrancken et al. [10], is similar for the XZ and

XY specimens, but the microstructure anisotropy is expected to be slightly more favourable towards resisting crack propagation in the case of the XY specimen. This analysis is consistent with the reported fracture toughness values for the AB specimens as function of specimen orientation.

After application of the stress relief heat treatment the fracture toughness values are within reasonable agreement for all the specimen orientations suggesting that the dominant residual stress effect argued above has been eliminated. Of course the columnar grain structure is still maintained, but the heat treatment may have sufficiently altered the planarity of the grain-to-grain interfaces to reduce the grain anisotropy effect. This detailed view of the microstructure and its influence on crack propagation remains to be investigated and is the topic of future research. In the case of the annealed HT condition, one might expect a similar agreement in the fracture toughness values for the respective orientations but, despite the overall increase in fracture toughness (Table 2), there is a 20% difference between the highest (XZ and ZX) and the lowest (XY) K_{1c} values. There are once again likely to be detailed microstructural aspects that might account for this behaviour, but the difference in K_{1c} values between the specimen orientations is substantially less than the 75% difference in the case of the AB specimens. Although annealing heat treatments offer the most favourable fracture toughness properties, it is once again reinforced in this study that the role of residual stresses, and consequently stress relief heat treatments, is critically important in influencing the competitiveness of parts produced by the SLM process. Knowles et al. [11] and Leuders et al. [7] have reported a substantial decrease in residual stress levels in SLM Ti6Al4V specimens after heat treatment (650ºC for 4 hours and 800ºC for 2

hours respectively). Leuders et al. [7] also concluded that higher temperature heat treatments did not provide any further favourable reduction in residual stress.

The fatigue crack growth rate (FCGR) behaviour very closely mimics the fracture toughness properties for the respective specimen orientations and process conditions. In the same way as for the fracture toughness values for the AB condition, the AB-XY specimen demonstrates the lowest FCGR (Figure 7(d)). The ZX and XZ specimens in the same condition have quite similar yet higher FCGR's. Correspondingly, there is more noticeable improvement in the FCGR resistance for the ZX and XZ specimens after heat treatment compared to the XY specimen, which if anything, displays slightly poorer FCGR resistance after heat treatment. Notwithstanding the fact that the more subtle influences of microstructure development as function of heat treatment remain to be investigated, the role of residual stress, and in particular the anisotropic influence of this residual stress, has been comprehensively accounted for in this study by comparing three different specimen orientations (relative to the build direction) and superimposing the influence of stress relief and annealing heat treatments.

Finally, the FCGR results from our study are compared to the results reported in the open literature (Figure 11).

Overall, there is a close correlation between the respective trend lines. For example, in the study by Leuders et al. [7] it is reported that the AB-ZX specimens possess the lowest FCGR resistance and there is a marked improvement with heat treatment. Of particular interest in Figure 11 is the inclusion of FCGR data for conventional wrought

Ti6Al4V [12]. The FCGR trendlines reported for SLM Ti6Al4V are not significantly different to the conventional wrought Ti6Al4V alloy.

5. Conclusions

The consideration of SLM build orientation and process condition has highlighted the sensitivity of mechanical properties to the anisotropic microstructural and residual stress effects that arise from the highly directional and rapid transient nature of the SLM manufacturing process. In particular, the following findings are highlighted:

- The effect of the relationship between build direction and fracture plane on the fracture toughness and fatigue crack growth rate is most noticeable when material is tested in the as-built condition and may be accounted for by the anisotropic residual stress distribution.
- Low temperature stress relief and annealing heat treatments improve fracture toughness and fatigue crack growth resistance relative to the as-built condition and at the same time contribute to the elimination of the influence of anisotropy.
- The uniaxial tensile properties are much less influenced by specimen orientation relative to build direction.

Acknowledgments

The main author acknowledges the Erasmus Mundus scholarship funded by the European Union. In addition, this work is based on the research supported in part by the National Research Foundation of South Africa (NRF) for the grant 80561 and the Agency for Innovation by Science and Technology (IWT) through the SBO-project

e-SHM (Belgium).

"Any opinion, finding and conclusion or recommendation expressed in this material is that of the authors and the NRF does not accept any liability in this regard".

References

1. B. Van Hooreweder, D. Moens, R. Boonen, J.P. Kruth, P. Sas, Analysis of Fracture Toughness and Crack Propagation of Ti6Al4V Produced by Selective Laser Melting, Advanced Engineering Materials. 14 (2012) 92-97.

2. L. Thijs, F. Verhaeghe, T. Craeghs, J. Van Humbeeck, J.P Kruth, A study of the microstructural evolution during selective laser melting of Ti6Al4V, Acta Mater. 58 (2010) 3303-3312.

3. J.P Kruth, M. Badrossamay, E. Yasa, J. Deckers, L. Thijs, J. Van Humbeeck, Part and material properties in selective laser melting of metals, Proceedings of the 16th International Symposium on Electromachining, Shanghai, China (2010).

4. E. Yasa, J. Deckers, J.P Kruth, M. Rombouts, J. Luyten, Experimental Investigation of Charpy Impact Tests on Metallic SLM Parts, Proceeding of the International Conference on Advanced Research in Virtual and Rapid Prototyping, Leiria, Portugal (2009) 207–214.

5. T. Vilaro, C. Colin, J.D Bartout, As-Fabricated and Heat-Treated Microstructures of the Ti-6Al-4V Alloy Processed by Selective Laser Melting Metall, Mater. Trans. 42A (2011) 3190‑3199.

6. P. Mercelis, J.P Kruth, Residual stresses in selective laser sintering and selective laser melting, Rapid Prototyping Journal. 12/5 (2006) 254‑265.

7. S. Leuders, M. Thone, A. Riemer, T. Niendorf, On the mechanical behaviour of titanium alloy TiAl6V4 manufactured by selective laser melting: Fatigue resistance and crack growth performance, International Journal of Fatigue. 48 (2013) 300-307.

8. B. Vrancken, L. Thijs, J.P Kruth, J. Van Humbeeck, Heat treatment of Ti6Al4V produced by Selective Laser Melting: Microstructure and mechanical properties, Journal of Alloys and Compounds. 541 (2012) 177‑185.

9. P. Rangaswamy, M.L Griffith, M.B Prime, T.M Holden, R.B Rogge, J.M Edwards, R.J Sebring, Residual stresses in LENS® components using neutron diffraction and contour method, Materials Science and Engineering. A399 (2005) 72–83.

10. B. Vrancken, V. Cain, R. Knutsen, J. Van Humbeeck, Residual Stress via the Contour Method in Compact Tension Specimens produced via Selective Laser Melting, Scripta Mater. 87 (2014) 29-32.

11. C.R Knowles, T.H Becker, R.B Tait, Residual stress measurements and structural integrity implications for selective laser melted Ti6Al4V, South African Journal of Industrial Engineering. 23 (2012) 119-129.

12. M.J Donachie, Titanium: A technical guide. ASM International, Materials Park, Ohio, USA, 1988.

Note: Please retain colors on figures supplied (4, 5, 6, 7 and 11)

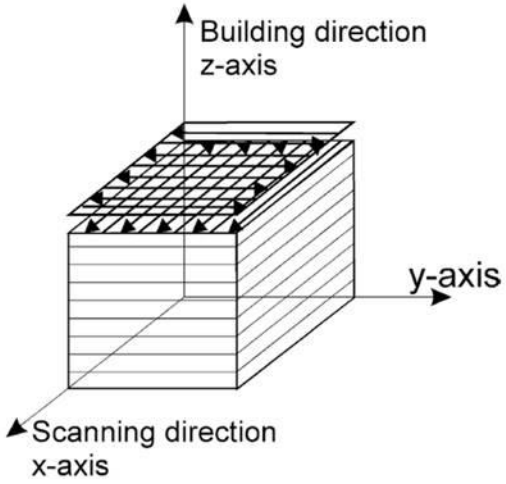

Figure 1: Scanning strategy (bi-directional) used to produce test specimens [2]

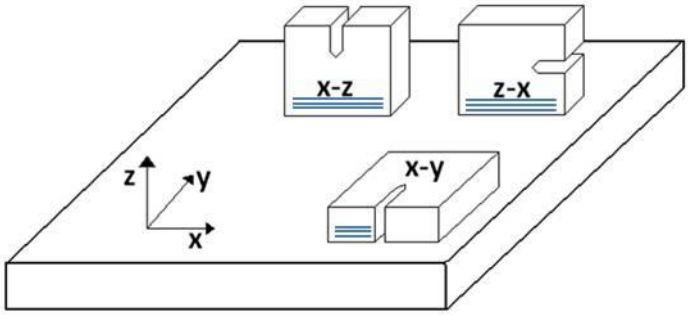

2(a)

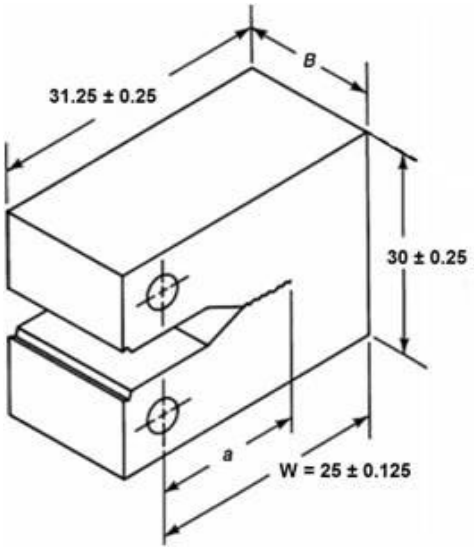

2(b)

Figure 2: (a) CT specimen orientations on the build-platform and (b) CT specimen geometry. The lines visible on (a) schematically represent the successive layers of powder.

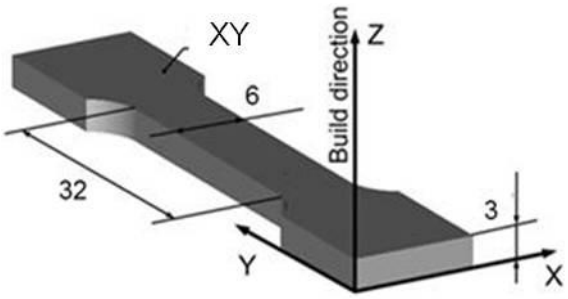

3(a)

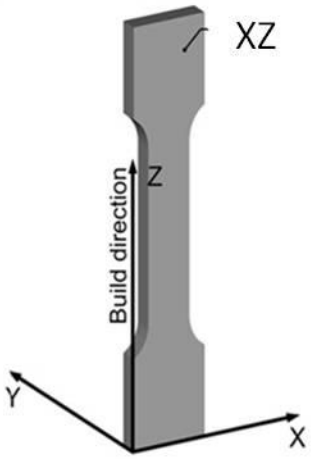

3(b)

Figure 3: Build orientation for XY and XZ tensile test specimens.

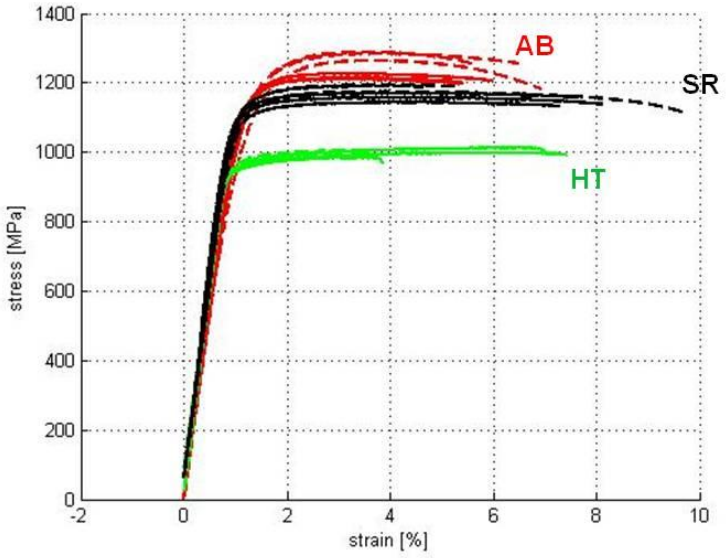

Figure 4: Tensile stress-strain curves for SLM-Ti6Al4V in the AB, SR and HT conditions. Dashed lines = XY and solid lines = XZ

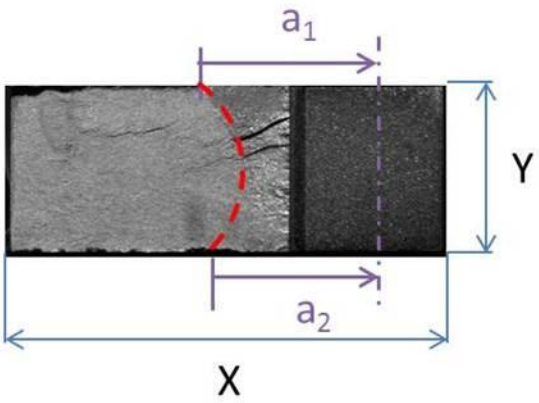

Figure 5: Uneven crack growth front for specimen ZX along the crack plane XY.

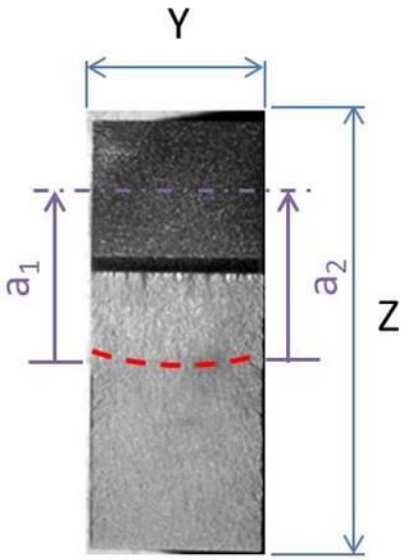

Figure 6: Thumbnail crack growth front for specimen XZ along the crack plane ZY.

Figure 7 is given in both JPEG and TIFF format

JPEG format

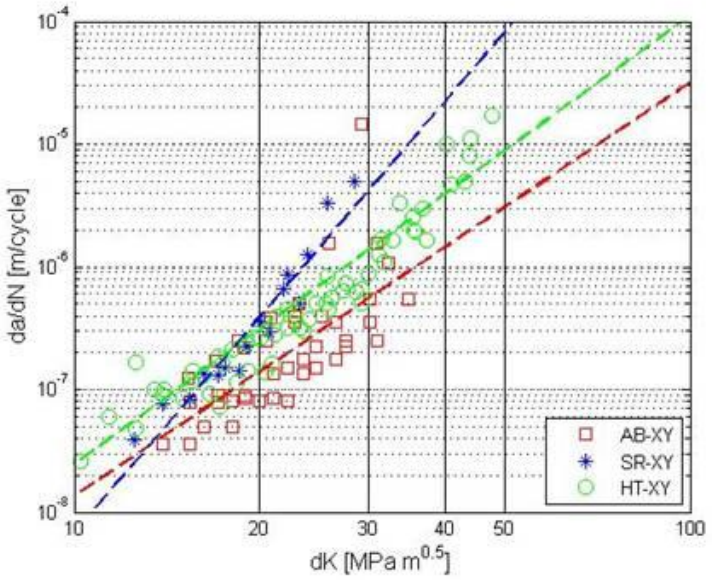

7(a)

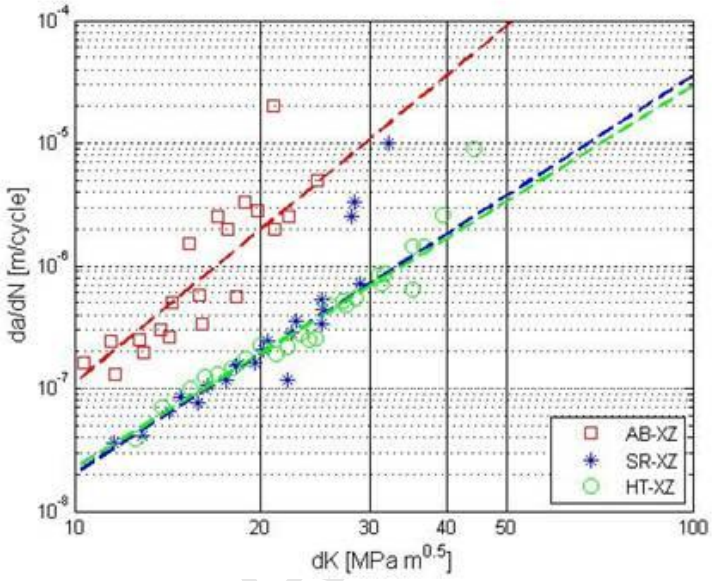

7(b)

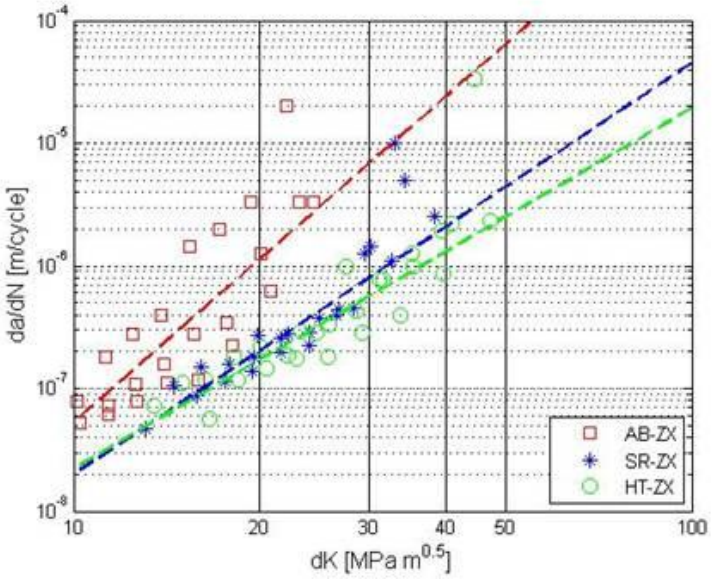

7(c)

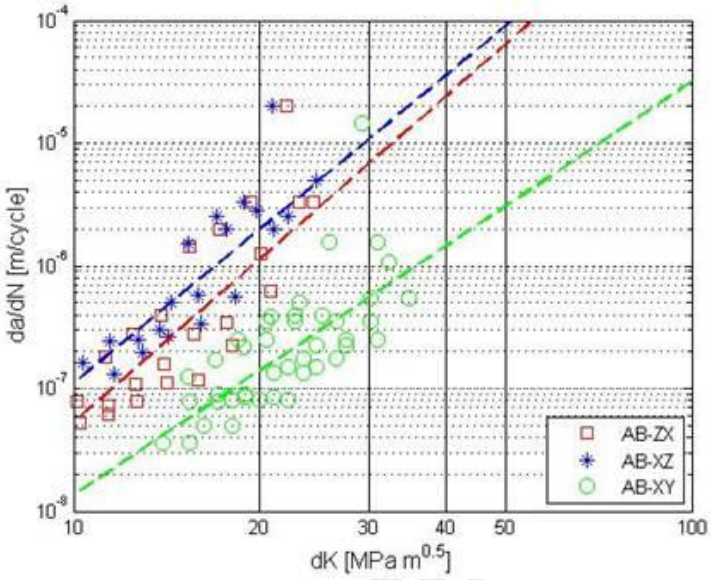

7(d)

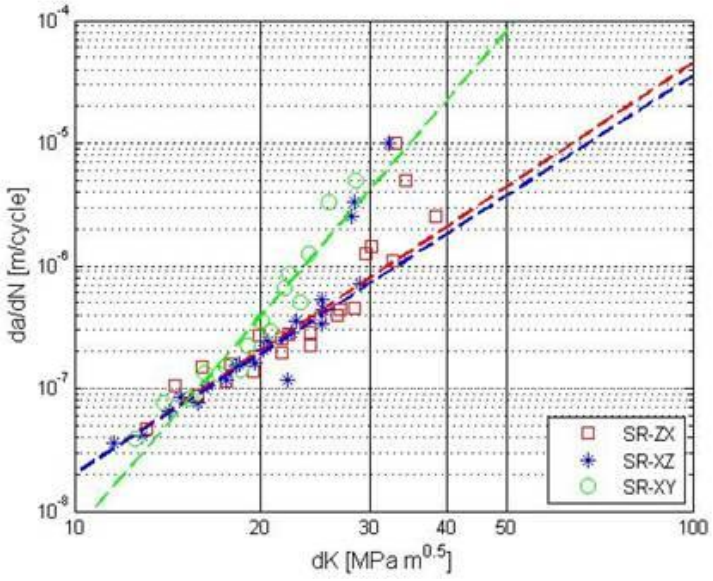

7(e)

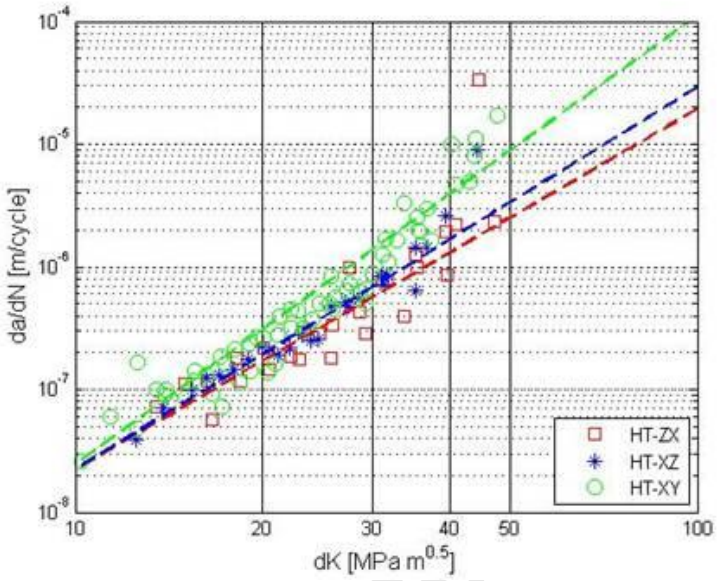

7(f)

Figure 7: Crack growth da/dN versus stress intensity range dK for (a) the XY specimen orientation, (b) the XZ specimen orientation, (c) the ZX specimen orientation, (d) the AB condition, (e) the SR condition and (f) the HT condition.

TIFF format

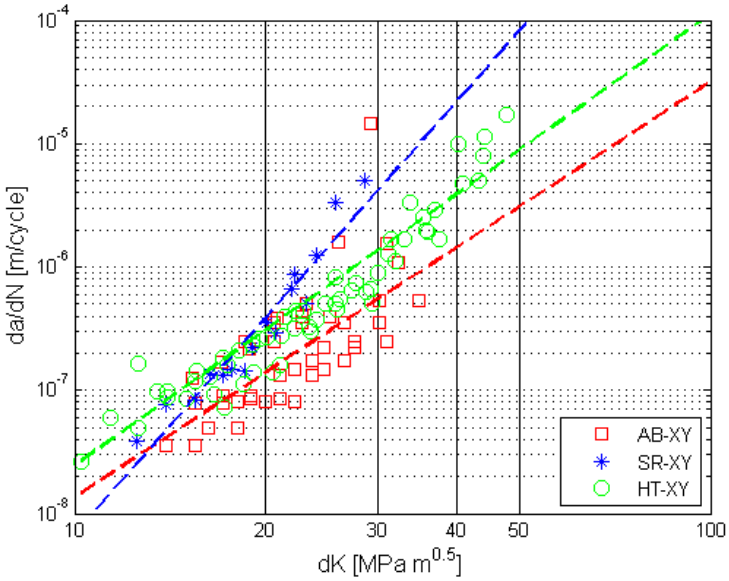

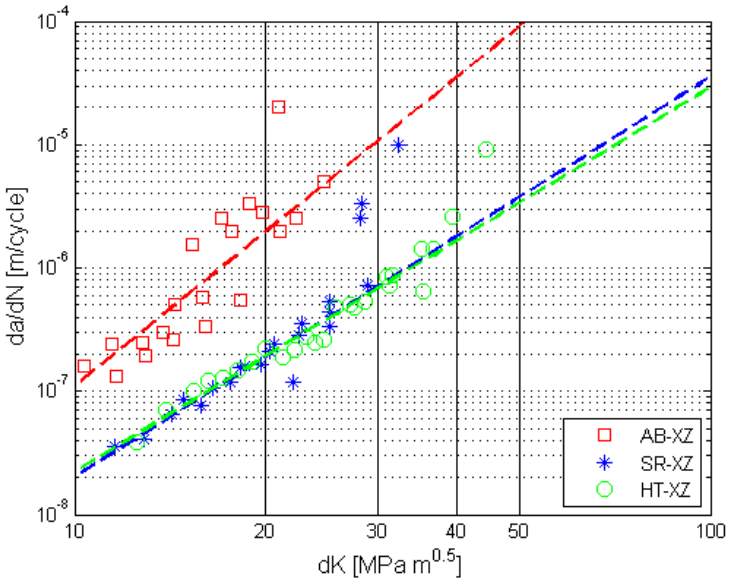

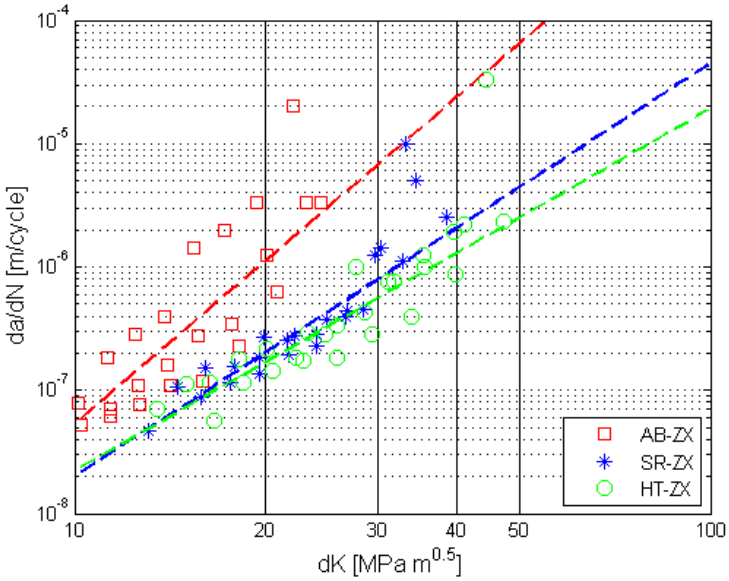

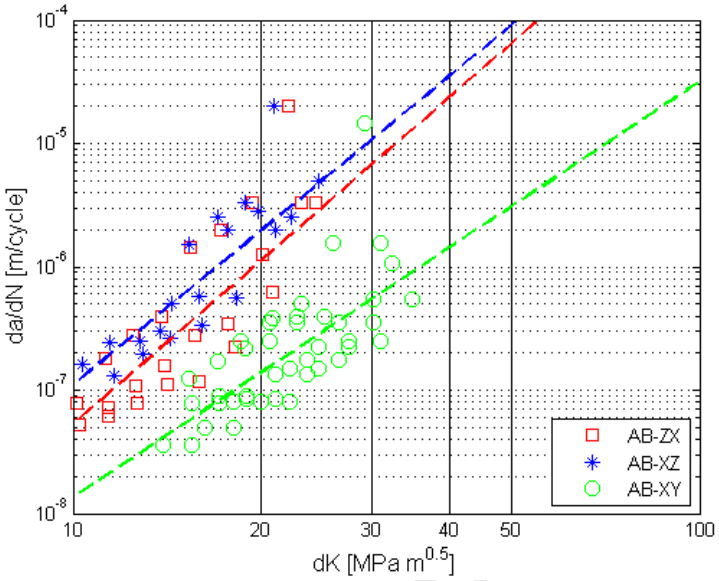

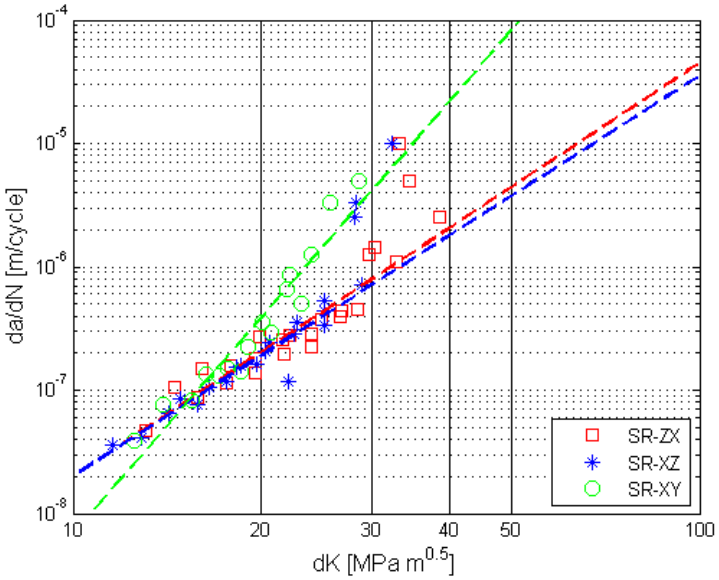

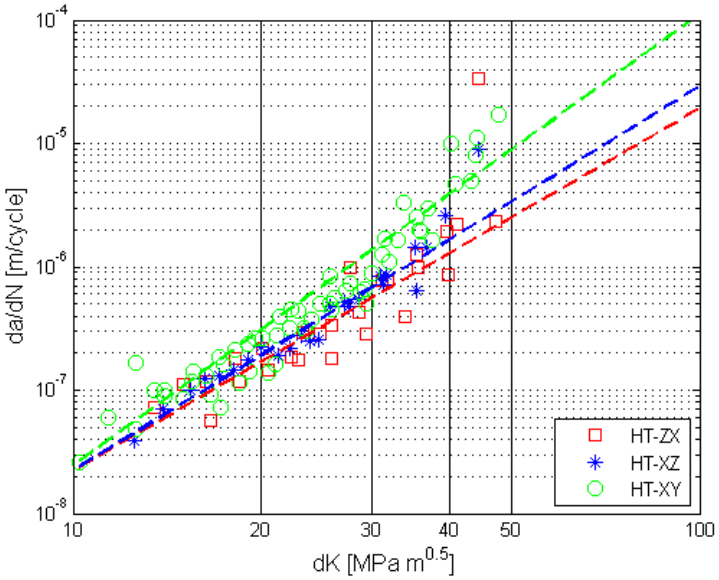

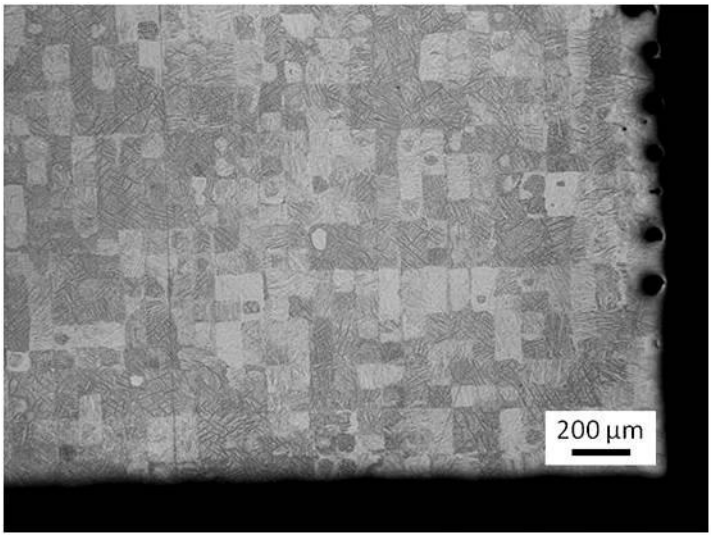

Figure 8: XY plane of SLM Ti6Al4V sample illustrating the checkerboard pattern.

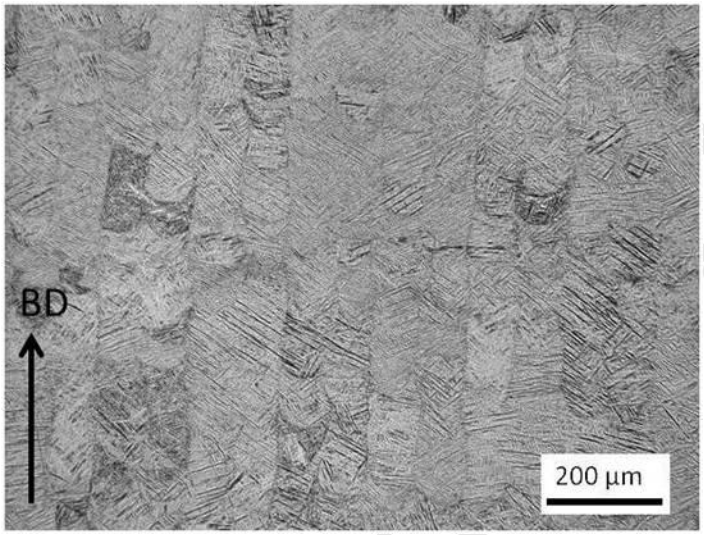

Figure 9: Columnar prior β grains in microstructure section parallel to SLM build direction (BD).

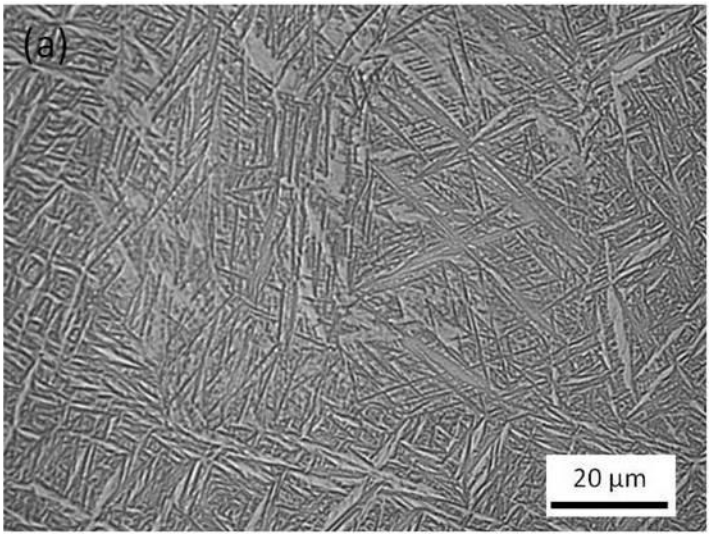

10(a)

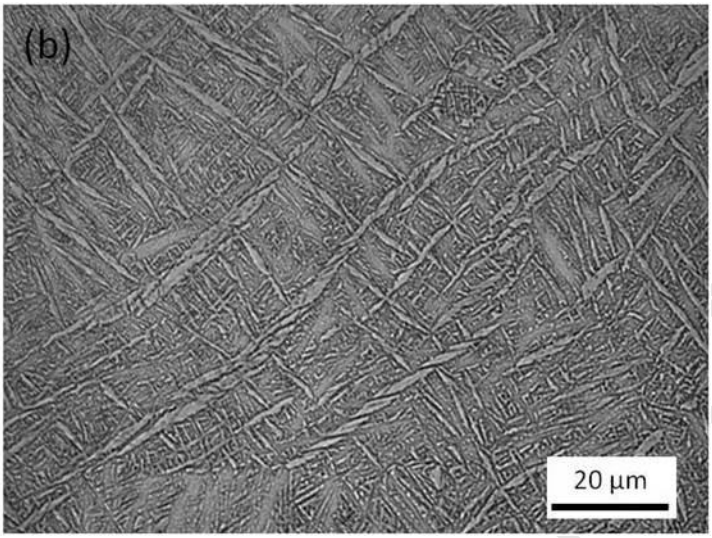

10(b)

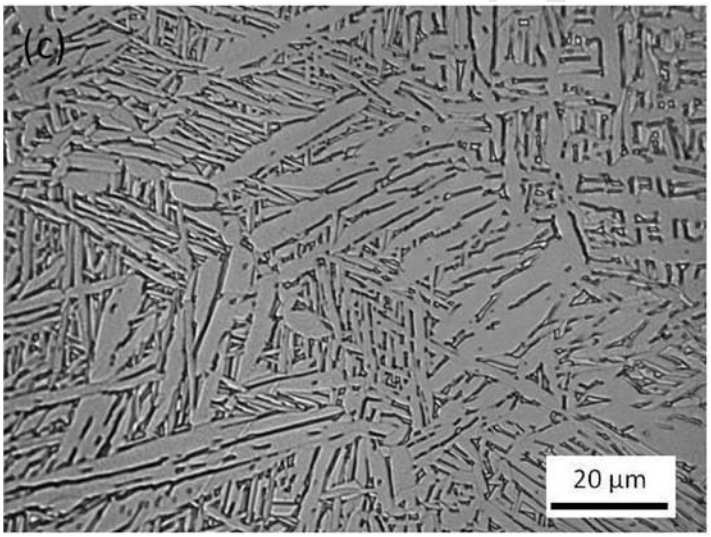

10(c)

Figure 10: Microstructure perpendicular to the build direction in the (a) AB condition, (b) SR condition and (c) HT condition.

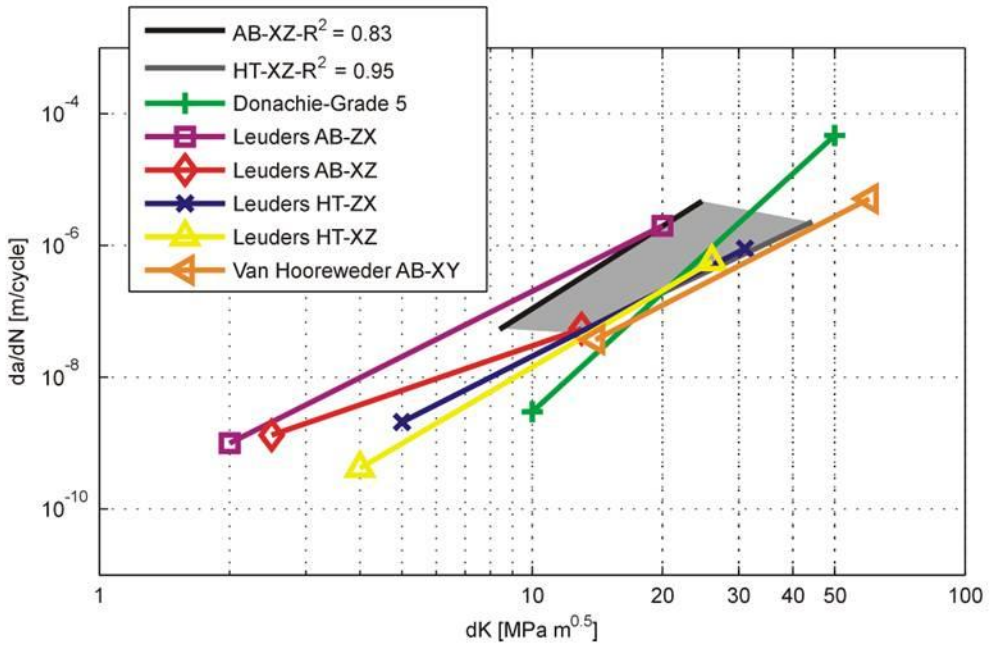

Figure 11: Comparison of slowest and fastest crack growth data with previous studies.

Table 1: Summary of tensile mechanical properties for AB, SR and HT specimens.

	σ_y [MPa]	σ_{UTS} [MPa]	ε_f [%]
AB (XY)	1093 ± 64	1279 ± 13	6 ± 0.7
AB (XZ)	1125 ± 22	1216 ± 8	6 ± 0.4
SR (XY)	1145 ± 17	1187 ± 10	7 ± 2.7
SR (XZ)	1132 ± 13	1156 ± 13	8 ± 0.4
HT (XY)	973 ± 8	996 ± 10	3 ± 0.4
HT (XZ)	964 ± 7	998 ± 14	6 ± 2

Table 2: Fracture toughness values for the as-built and heat treated XY, XZ and ZX specimen orientations.

K_{1c} (MPa.$m^{½}$)	XY	XZ	ZX
AB	28 ± 2	23 ± 1	16 ± 1
SR	28 ± 2	30 ± 1	31 ± 2
HT	41 ± 2	49 ± 2	49 ± 1

Table 3: Paris parameters and relevant correlation factors

	m	**C (m.cycle)**	**R^2**
XY-AB	3,37	5,79E-12	0.74
XY-HT	3,83	2,04E-12	0.91
XY-SR	5,84	9,93E-15	0.91
XZ-AB	4,17	7,51E-12	0.84

XZ-HT	3,11	1,71E-11	0.95
XZ-SR	3,24	1,16E-11	0.93
ZX-AB	4,41	2,08E-12	0.78
ZX-HT	2,94	2,58E-11	0.87
ZX-SR	3,35	8,85E-12	0.90